HHS Public Access

Author manuscript

J Med Chem. Author manuscript; available in PMC 2017 December 08.

Published in final edited form as:

J Med Chem. 2016 December 08; 59(23): 10619–10628. doi:10.1021/acs.jmedchem.6b01161.

Sulfonamide-Based Inhibitors of Aminoglycoside Acetyltransferase Eis Abolish Resistance to Kanamycin in *Mycobacterium tuberculosis*

Atefeh Garzan[†], **Melisa J. Willby**[‡], **Keith D. Green**[†], **Chathurada S. Gajadeera**[†], **Caixia Hou**[†], **Oleg V. Tsodikov**[*,†], **James E. Posey**[*,‡], and **Sylvie Garneau-Tsodikova**[*,†]

[†]University of Kentucky, Department of Pharmaceutical Sciences, College of Pharmacy, 789 South Limestone St., Lexington, Kentucky 40536-0596, United States

[‡]Mycobacteriology Laboratory Branch, Division of Tuberculosis Elimination, National Center for HIV/AIDS, Viral Hepatitis, STD, and TB Prevention, Centers for Disease Control and Prevention, Atlanta, Georgia 30333, United States

Abstract

A two-drug combination therapy where one drug targets an offending cell and the other targets a resistance mechanism to the first drug is a time-tested, yet underexploited approach to combat or prevent drug resistance. By high-throughput screening, we identified a sulfonamide scaffold that served as a pharmacophore to generate inhibitors of *Mycobacterium tuberculosis* acetyltransferase Eis, whose upregulation causes resistance to the aminoglycoside (AG) antibiotic kanamycin A (KAN) in *Mycobacterium tuberculosis*. Rational systematic derivatization of this scaffold to maximize Eis inhibition and abolish the Eis-mediated KAN resistance of *M. tuberculosis* yielded several highly potent agents. A crystal structure of Eis in complex with one of the most potent inhibitors revealed that the inhibitor bound Eis in the AG-binding pocket held by a conformationally malleable region of Eis (residues 28–37) bearing key hydrophobic residues. These Eis inhibitors are promising leads for preclinical development of innovative AG combination therapies against resistant TB.

[*]Corresponding Authors: For S.G.-T.: phone, 859-218-1686; sylviegtsodikova@uky.edu. For J.E.P.: phone, 404-639-1712; jposey@cdc.gov. For O.V.T.: phone, 859-218-1687; oleg.tsodikov@uky.edu.

Accession Codes

Coordinates and structure factor amplitudes for the Eis-CoA-inhibitor **39** complex have been deposited in the Protein Data Bank under accession code 5IV0. Authors will release the atomic coordinates and experimental data upon article publication.

Author Contributions

All authors designed the experiments. A.G. performed all chemical synthesis and determined IC_{50} values for the synthesized compounds **29**–**47**. M.J.W. determined all MIC values in *Mtb* strains. K.D.G. performed HTS and determined the original IC_{50} values for compound **29** following HTS. C.S.G. and C.H. performed crystallization of the Eis-CoA-inhibitor **39** ternary complex. O.V.T. determined the Eis-CoA-inhibitor **39** ternary complex crystal structure. A.G., M.J.W., K.D.G., O.V.T., J.E.P., and S.G.-T. analyzed data. A.G., O.V.T., J.E.P., and S.G.-T. wrote the manuscript. A.G. and M.J.W. contributed equally to this work.

The authors declare no competing financial interest.

Supporting Information

The Supporting Information is available free of charge on the ACS Publications website at DOI: 10.1021/acs.jmed-chem.6b01161.

Figures showing HPLC traces, representative dose–response data, and the structure of Eis in complex with inhibitor **39** overlaid with TOB and inhibitor **13g** from a previous study (PDF)

Molecular formula strings (CSV)

Graphical Abstract

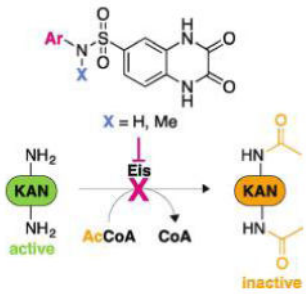

INTRODUCTION

Tuberculosis (TB) is an infectious disease caused by *Mycobacterium tuberculosis* (*Mtb*) that leads to ~1.5 million deaths globally each year.[1] Because of the spread of multidrug-and extensively drug-resistant (MDR- and XDR-) strains of *Mtb*, new therapeutic strategies are needed. The aminoglycosides (AGs) kanamycin A (KAN) and amikacin (AMK) are used to treat MDR- and possibly XDR-TB, but resistance to these agents occurs as well. An important mechanism of TB resistance to the AG KAN is the upregulation of the enhanced intracellular survival (*eis*) gene.[2–4] We previously demonstrated that the *Mtb* Eis protein (Eis_*Mtb*) is an acetyltransferase capable of multiacetylating a variety of AGs,[5] including the TB therapeutics KAN and AMK, via a random sequential mechanism,[6] thereby abolishing the antibiotic activity of these drugs. The ability to acetylate an AG molecule at multiple amine positions due to its unique structure distinguishes Eis from other AG acetyltransferases (AACs), which are known to be exquisitely regiospecific. A crystal structure of Eis_*Mtb* in complex with coenzyme A and tobramycin (TOB) demonstrated how TOB could interact with the Eis active site in two binding modes for the observed diacetylation of the 6′- and 3″-amines of this AG.[7]

Multiacetylation by Eis has a defined pattern for each AG: the number of acetylations and the positions of the amino groups that get acetylated depend on the structure of the AG.[7] Furthermore, we showed that Eis homologues from *Mycobacterium smegmatis*,[8] *Mycobacterium abscessus*,[9] *Anabaena variabilis*,[10] *Bacillus anthracis*,[11] *Gordonia bronchialis*,[9] *Kocuria rhizophila*,[9] and *Tsukamurella paurometabola*[9] are also functional AACs, which exhibit differences in regiospecificity and can be inhibited by chlorhexidine, a nonclinically relevant Eis_*Mtb* inhibitor.[12] In addition to AG substrate versatility, Eis enzymes display some acyl-CoA cosubstrate promiscuity[13] and can acetylate non-AG molecules containing lysine residues, such as capreomycin[14] and the JNK-specific dual-specificity protein phosphatase 16 (DUSP16)/mitogen-activated protein kinase phosphatase-7 (MKP-7) pair.[15] These observations underscore the uniqueness and versatility of Eis AG modifying activity and its high capacity for inactivation of diverse AG drugs.

The development of AGs that cannot be modified by Eis or a novel therapy that would involve an Eis inhibitor used in combination with KAN are two possible approaches to overcome resistance caused by *eis* upregulation in *Mtb*. The former route is complicated by the ability of Eis to accept structurally diverse AGs as substrates, whereas the latter route is

potentially more suitable. With a similar idea applied to β-lactam inactivating enzymes, Blanchard and co-workers showed that meropenem in combination with a β-lactamase inhibitor clavulanic acid act synergistically in killing *Mtb* in vitro and in mice.[16] We previously reported that some Eis inhibitors displayed AG-competitive and mixed modes of action, establishing a proof of principle for inhibition of Eis in vitro.[12] Recently, we additionally discovered and optimized three lead scaffolds of inhibitors of *Mycobacterium tuberculosis* (*Mtb*) acetyltransferase Eis from high-throughput screening (HTS).[17,18]

Here, we report the discovery and rational structure-based optimization via medicinal chemistry of promising sulfonamide Eis inhibitors that not only efficiently inhibit the purified enzyme, but also restore KAN susceptibility of KAN-resistant *Mtb*. We also present a crystal structure of Eis in complex with CoA and one potent sulfonamide inhibitor, which reveals its mode of action, explains our SAR study, and paves the way for further rational structure-based development of Eis inhibitors.

RESULTS AND DISCUSSION

Identification and Chemical Synthesis of Eis Inhibitors

To identify potential Eis inhibitor candidates, we used an established UV absorbance-based HTS assay[12] to screen over 123000 structurally diverse small molecules for their inhibition of KAN acetylation by the Eis_*Mtb* acetyltransferase in vitro. The screening of this molecular library against Eis_*Mtb* led to the identification of a sulfonamide scaffold (Figure 1A). The HTS library contained 29 compounds (**1**–**29**) with this core structure, and four (**1**, **3**, **4**, and **29**) were identified as hits (i.e., compounds displaying ≥3-fold higher inhibition than the magnitude of the standard deviation). Compounds **2** and **5**–**28** were found not to inhibit Eis in the HTS. As compounds **16**–**28** were unable to inhibit Eis, we concluded that at least an aromatic ring attached to the nitrogen atom is important for inhibitory activity. While compounds **1**, **3**, and **4** displayed modest Eis inhibition, compound **29** potently inhibited Eis activity (IC_{50} = 0.5 ± 0.1 μM). On the basis of this encouraging result, we synthesized compound **29** along with 18 additional sulfonamide analogues (**30**–**47**) containing a variety of substituents on the aniline ring to define a preliminary body of structure–activity relationship (SAR) of Eis inhibition. The compounds were synthesized by a reaction of 2,3-dihydrox-yquinoxaline with chlorosulfonic acid to generate sulfonyl chloride, which then reacted with different aniline derivatives to yield compounds **29**–**47** (Figure 1B).

Biochemical and Biological Testing of Sulfonamides 29–47

To investigate the potential of these compounds as Eis inhibitors for use in combination with KAN, we evaluated their biochemical (IC_{50} values against purified Eis enzyme) and biological (effect on the MIC values of KAN in KAN-sensitive *Mtb* H37Rv and in KAN-resistant *Mtb* K204[2]) properties in parallel studies (Table 1 and Supporting Information, Figure S20). Importantly, *Mtb* K204 is genetically identical to H37Rv, except for one clinically derived point mutation in the *eis* promoter that causes upregulation of Eis acetyltransferase, resulting in the resistance of *Mtb* K204 to KAN.[2] In this regard, H37Rv serves as an important Eis knockdown control for validating the mechanism of action of the

Eis inhibitors in the bacterial cell. To correct out the effect of different potencies (IC_{50}) of the Eis inhibitors as determined by the enzyme assay, in the MIC assays we used the inhibitors at concentrations that were 100-fold higher than their IC_{50} values, where achievable. The freshly synthesized compound **29** displayed robust inhibition of Eis in vitro (IC_{50} = 0.08 ± 0.02 μM). When combined with KAN, sulfonamide **29** resulted in a 4-fold reduced KAN MIC value (2.5 μg/mL) compared to KAN alone (10 μg/mL) for K204 *Mtb*. This was a reduction almost to the MIC level of KAN in the KAN-susceptible *Mtb* H37Rv (1.25 μg/mL) parent strain. To gain insight into the importance of the substitution pattern on the aniline portion of the sulfonamide scaffold, we generated secondary (NHAr) and tertiary (N(Me)Ar) sulfonamides (**29**–**47**). Eis inhibition assays with the synthesized sulfonamides were carried out in combination with KAN. The nonmethylated counterpart of lead compound **29**, compound **30**, displayed lower Eis inhibitory activity (IC_{50} = 6.24 ± 1.31 μM) and had a smaller effect than **29** did on the KAN resistance in *Mtb* K204 (MIC_{KAN} = 5 μg/mL). Two other nonmethylated derivatives, **32** and **34**, also resulted in lower Eis inhibitory activity (IC_{50} > 200 and 10.6 ± 2.5 μM, respectively) and did not overcome KAN resistance in *Mtb* K204 (MIC_{KAN} = 10 and 5 μg/mL, respectively). These data, in conjunction with the fact that compounds **1** and **3**–**13** from the HTS did not display significant Eis inhibition, suggest that the *N*-methyl group is essential for efficient Eis inhibition and antitubercular activity.

Having established the importance of the *N*-methyl moiety, we explored the effect of substitutions on the benzene ring of the aniline moiety. Removing all substituents on the benzene ring (compound **31**) resulted in a 70-fold decrease in Eis inhibitory activity (IC_{50} = 5.8 ± 1.8 μM) when compared to that of lead **29** and did not overcome KAN resistance in *Mtb* K204, suggesting the importance of a substituted aniline for Eis inhibition and antimycobacterial activity. In general, *para* substitution (compounds **29** with a *p*-Br, **33** with a *p*-*i*Pr, and **35** with a *p*-Cl) was found to be favorable and yielded compounds with IC_{50} values varying from 0.08 to 0.25 μM, which overcame KAN resistance (MIC_{KAN} = 2.5 μg/mL) in KAN-resistant *Mtb*. Interestingly, *p*-methoxy substitution resulted in a compound (**14**) that was found to be inactive during our HTS. To delineate if *ortho* or *meta* substitution would be more favorable than *para* substitution, we generated compounds **36** (with an *o*-OMe) and **39** (with a *m*-OMe). The *o*-methoxy substituted **36** was found to be completely inactive (IC_{50} > 200 μM and MIC_{KAN} = 10 μg/mL against *Mtb* K204), whereas the *m*-methoxy substituted **39** was found to be a potent Eis inhibitor (IC_{50} = 5.8 ± 1.2 μM) and was one of our two compounds to fully overcome KAN resistance in *Mtb* K204 (MIC_{KAN} ≤ 1.25 μg/mL). It is important to note that incorporating an additional *m*-methoxy group, as in compound **40**, was detrimental for the overall activity of the molecule, which suggested that monosubstitution is more promising than disubstitution. We also synthesized the *m*-bromo derivative **38**, which demonstrated a slightly improved Eis inhibitory activity (IC_{50} = 0.056 ± 0.004 μM) than did the corresponding *para* derivative **29** while also being able to overcome KAN resistance in *Mtb* K204 (MIC = 2.5 μg/mL). We also found that the *m*-isopropyl derivative **43** and its *para* counterpart **33** displayed similar Eis inhibitory activity (IC_{50} = 0.23 ± 0.03 and 0.25 ± 0.06 μM, respectively) and resulted in identical KAN MIC values (2.5–5 μg/mL) against KAN-resistant *Mtb*. While the *p*-methyl derivative **15** was inactive in our HTS, its *meta* counterpart **41** displayed good Eis inhibition (IC_{50} = 0.37

± 0.09 μM) and some ability to overcome KAN resistance in *Mtb* K204 (MIC 2.5–5 μg/mL). These data suggest that mono-*meta* substitution is either equal or more advantageous then *para*, which is more beneficial than *ortho*. On the basis of these results, we generated additional *m*-alkylated sulfonamides (**42**, **44**, and **45**) and observed that longer or bulkier alkyl groups, although good for Eis inhibition, did not produce compounds capable of overcoming KAN resistance in *Mtb* K204. Finally, with the hope of increasing any possible π–π interaction between the inhibitor and the AG-binding site of the *Mtb* Eis, we generated compound **46**, which showed a dramatic increase in Eis inhibitory activity (IC_{50} = 0.00024 ± 0.00010 μM) and was found to completely overcome KAN resistance in *Mtb* K204 ($MIC_{KAN} \leq 1.25$ μg/mL). Compound **46** is currently our most potent and promising Eis inhibitor that can be used in conjunction with KAN. Because compound **39** with the methoxy group in the *meta* position is one of our best compounds to fully overcome KAN resistance in *Mtb* K204, we also synthesized compound **47** with a *m*-methoxy substitution on the naphthyl group, but this led both to a loss of Eis inhibition and to a loss of the effect on MIC_{KAN} (see next section).

The Eis inhibitors lacked anti-*Mtb* activity in the absence of KAN in either tested strain (Table 1). Furthermore, most compounds sensitized the KAN-resistant *Mtb* K204 to KAN, as expected based on their 100-fold IC_{50} concentrations used in these assays, with two compounds (**39** and **46**) completely canceling the effect of the Eis upregulation in *Mtb* K204. The two compounds that were least potent in the enzymatic assay (**32** and **36**) and used in the MIC assay at concentrations below 100 × IC_{50} were also inert in that assay. This general correlation of the potency in the enzymatic assays and their effect on MIC_{KAN} canceling that of Eis upregulation, taken together, validate inhibition of Eis by these compounds as the mechanism of their sensitization of *Mtb* K204 to KAN. Synergistic growth inhibition in combination with KAN by some effect other than Eis inhibition can be ruled out because the inhibitors do not change MIC_{KAN} in H37Rv. The cell envelope of *Mtb* is a notoriously tough barrier, and some compounds penetrate the cell envelope more readily than others in a manner that is not correlated with the IC_{50} values. This would explain the variability of MIC_{KAN} values in Table 1.

To examine the selectivity of our two best inhibitors (**39** and **46**) toward Eis, we next tested these two compounds against three other AAC enzymes: AAC(2′)-Ic from *Mtb*,[19,20] AAC(3)-IV from *Escherichia coli*,[21,22] and AAC(6′)-Ie/APH(2″)-Ia from *Staphylococcus aureus*.[23,24] Sulfonamides **39** and **46** did not inhibit KAN acetylation by the AACs tested at concentrations as high as 200 μM, with the exception of **39**, which inhibited 15% of the AAC(2′)-Ic activity when tested at 200 μM. These data demonstrate the high selectivity of our inhibitors toward Eis.

Crystal Structure of EisC204A-CoA-Inhibitor 39 Complex

To characterize the mechanism of our Eis inhibitors, explain the SAR, and aid in future drug development, we determined the crystal structure of Eis in complex with CoA and inhibitor **39** at the resolution of 2.1 Å (Figure 2 and Table 2). Although sulfonamide **46** was our best compound in biochemical and biological studies, it did not cocrystallize with Eis. The crystal structure demonstrates that inhibitor **39** is bound in the part of the AG-binding pocket

that is formed by the N-terminal domain of Eis. The inhibitor binding site partially overlaps with the binding site of TOB, as observed in our previously reported structure of Eis-CoA-TOB (Supporting Information, Figure S21),[7] indicating that the Eis inhibitors are competitive with AGs. The inhibitor is apparently stabilized in the bound state by numerous hydrophobic interactions (Figure 2B,C). The shape of the inhibitor binding pocket and the interacting hydrophobic residues are not conserved in other AAC enzymes, explaining the observed selectivity of the inhibitors. Specifically, the aniline moiety is stacked between the rings of Phe84 and Trp36, with the methoxy group located in the hydrophobic pocket lined by the nonpolar stem of the Arg37 side chain, Phe84, Trp13, and Leu63. This explains why removing the aniline ring resulted in a loss of activity for compounds **13**, **16**, **17**, and **23**–**27**. The quinoxalinedione moiety stacks against Phe24, a residue that also interacts with TOB (Supporting Information, Figure S21B), as previously observed in a crystal structure of an Eis-TOB complex (Supporting Information, Figure S21).[7] The NH group of the quinoxalinedione ring on the side of the sulfonamide forms a hydrogen bond with the carboxyl group of Asp26 (N–O distance of 2.7 Å), and the oxygen of the sulfonamide forms a hydrogen bond with the main chain nitrogen of Ile28 (O–N distance of 3.0 Å). Our SAR studies showed that compounds with an *N*-methyl group of the sulfonamide moiety displayed higher Eis inhibitory activity than those with an NH group, which can be rationalized by the optimal van der Waals interaction of the methyl with Trp36 (the distance between the methyl C atom and the closest C of the Trp36 side chain is 3.6 Å). Eliminating the methyl group would abolish this interaction, putting a polar NH in a hydrophobic environment, likely destabilizing binding (**6** vs **37**, **30** vs **29**, **32** vs **31**, and **34** vs **33**). Replacing the aniline ring with an *N*-aryl piperazine (compounds **18**–**22**) resulted in a loss of Eis inhibitory activity when compared to the aniline ring. As described above, this part of the molecule is snugly fit in a hydrophobic pocket, which is too small to accommodate these larger groups. The *ortho* position of the aniline ring is flanked by the C-terminal residue Phe402 and it abuts Phe84, explaining why an *ortho* substitution, as in compound **36**, resulted in a loss of Eis inhibitory activity. A bulky group such as *n*-butyl (**44**) or *t*-butyl (**45**) in *meta* position of the aniline ring would clash with Arg37 that is structurally fixed by π–π stacking with the inhibitor, explaining the poor inhibitory activity of these two compounds. A *meta*,*meta*-disubstitution (**40**) resulted in a dramatic decrease in activity as the second substituent would clash with the side chain of Met65. Electron-donating groups such as methoxy (**39**) or a naphthalene ring (**46**) increase the π–π interaction of the aniline ring with Phe84 and Trp36, explaining their stronger interactions in the AG-binding pocket of Eis. However, combining the two substituents in compound **47** led to a loss of activity, as both substitutions cannot be sterically accommodated.

The overall conformation of Eis in complex with the inhibitor is similar to the previously reported crystal structure.[5] A notable conformational difference is that a part of a loop (residues 28–30) and a helix (residues 31–37) are shifted toward the inhibitor relative to their conformation in the structure without the inhibitor by 1–1.5 Å, apparently in an induced-fit fashion, to maximize steric contacts. The indole ring of Trp36 in this helix is rotated by ~40°, maximizing the stacking with the aniline ring and other interactions, as explained above. These small, but significant conformational changes likely precluded us from obtaining a correct model of a bound inhibitor by prior extensive computational docking

simulations. Inhibitor **39** occupies a similar space in the AG binding pocket as a previously reported inhibitor with the isothiazole *S,S*-dioxide heterocyclic core (labeled **13g** in ref 17) (Supporting Information, Figure S21), but the orientations of the two inhibitors and their interactions with the protein side chains are largely different. The only common feature is the nearly coplanar binding of the methoxy- and the chlorophenyl rings of the two respective inhibitors, with both rings sandwiched by Phe84 and Trp36 of Eis (Supporting Information, Figure S21B). In summary, the crystal structure of the EisC204A-CoA-inhibitor **39** complex allowed us to fully explain our biochemical and biological data and provides a solid foundation for further rational structure-based development of Eis inhibitors.

CONCLUSION

In conclusion, the biochemical, biological, and structural studies described in this manuscript provide a proof-of-principle of the activity of Eis inhibitors as promising KAN adjuvants. The SAR combined with the cocrystal structure will guide future development of these compounds for their clinical use against MDR- and XDR-TB.

EXPERIMENTAL SECTION

Chemistry

General—All reagents were purchased from commercial sources and used without purification. TLC analyses were performed on silica gel plates 60 F254 (precoated on glass; 0.20 mm thickness with fluorescent indicator UV_{254}) and were visualized by UV or charring in $KMnO_4$ stain. ^1H and ^{13}C NMR spectra were collected on a 400 MHz NMR spectrometer (VARIAN INOVA) using $(CD_3)_2SO$. Chemical shifts are reported in parts per million (ppm) and are referenced to residual solvent peaks. All reactions were conducted under nitrogen atmosphere, and all yields reported refer to isolated yields. The known compound 2,3-dihydroxy-6-quinoxalinesulfonyl chloride was characterized by ^1H NMR and is in complete agreement with sample reported elsewhere. All new compounds were characterized by ^1H, ^{13}C NMR, and mass spectrometry. Further confirmation of purity for these final molecules was obtained by RP-HPLC, which was performed on an Agilent Technologies 1260 Infinity HPLC system by using the following general method 1: Flow rate = 1 mL/min; λ = 254 nm; column = Vydac 201SP C18, 250 mm × 4.6 mm, 90A 5 μm. Eluents: A = H_2O + 0.1% TFA, B = MeCN. Gradient profile: starting from 5% B, increasing from 5% B to 100% B over 20 min, holding at 100% B from 20 to 27 min, decreasing from 100% B to 5% B from 27 to 30 min. Prior to each injection, the HPLC column was equilibrated for 15 min with 5% B. All compounds were ≥95% pure.

Synthesis and Characterization of Sulfonamides Generated in This Study. 2,3-Dihydroxy-6-quinoxalinesulfonyl Chloride: The known compound 2,3-dihydroxy-6-quinoxalinesulfonyl chloride was prepared following a previously published protocol.[25] Chlorosulfonic acid (20.53 mL, 308.36 mmol) was added to quinoxaline-2,3-diol (5.00 g, 30.83 mmol). The reaction mixture was then refluxed for 12 h. After cooling to room temperature, the reaction mixture was carefully poured onto ice and filtered, and the precipitate was washed with H_2O (50 mL). The solid was collected and recrystallized with toluene to afford 2,3-dihydroxy-6-quinoxalinesulfonyl chloride (7.07 g, 88%) as a white

solid. ^{1}H NMR (400 MHz, $(CD_3)_2SO$, which matches lit.[25]) δ 11.97 (s, 1H), 11.94 (s, 1H), 7.43 (d, J = 1.6 Hz, 1H), 7.30 (dd, J = 8.4, 1.6 Hz, 1H), 7.04 (d, J = 8.4 Hz, 1H).

General Procedure for the Synthesis of Sulfonamides (e.g., N-(4-Bromophenyl)-N-methyl-2,3-dioxo-1,2,3,4-tetrahydro-6-quinoxalinesulfonamide (29)—A solution of 2,3-dihydroxy-6-quinoxalinesulfonyl chloride (0.30 g, 1.15 mmol) and 4-bromo-*N*-methylaniline (0.29 mL, 2.30 mmol) in DMF (6 mL) was stirred at room temperature for 12 h. H_2O was added to the reaction mixture, and the formed precipitate was filtered and washed with H_2O (10 mL) to yield **29** (0.21 g, 45%) as a purple solid. ^{1}H NMR (400 MHz, $(CD_3)_2SO$) δ 12.27 (s, 1H), 12.00 (s, 1H), 7.55 (app dt, J = 9.6, 3.2 Hz, 2H), 7.25 (d, J = 9.6 Hz, 2H), 7.24 (s, 1H), 7.07 (app dt, J = 9.2, 3.2 Hz, 2H), 3.09 (s, 3H). ^{13}C NMR (100 MHz, $(CD_3)_2SO$) δ 155.2, 154.8, 140.4, 131.9, 129.8, 129.3, 128.4, 125.9, 122.4, 120.2, 115.5, 114.4, 37.7. LRMS m/z calcd for $C_{15}H_{13}BrN_3O_4S$ $[M + H]^+$ 410.0; found 410.8. Purity of the compound was further confirmed by RP-HPLC by using method 1: R_t = 8.77 min (98% pure; Supporting Information, Figure S1).

N-(4-Bromophenyl)-2,3-dioxo-1,2,3,4-tetrahydro-6-quinoxalinesulfonamide (30): As described for the synthesis of compound **29**, 2,3-dihydroxy-6-quinoxalinesulfonyl chloride (0.30 g, 1.15 mmol), 4-bromoaniline (0.39 g, 2.30 mmol), and DMF (6 mL) were used to afford compound **30** (0.21 g, 47%) as a light-yellow solid. ^{1}H NMR (400 MHz, $(CD_3)_2SO$) δ 12.17 (s, 1H), 12.09 (s, 1H), 10.49 (br s, 1H), 7.51 (d, J = 1.6 Hz, 1H), 7.45 (dd, J = 8.0, 1.6 Hz, 1H), 7.41 (app dt, J = 9.6, 2.8 Hz, 2H), 7.19 (d, J = 8.0 Hz, 1H), 7.04 (app dt, J = 9.6, 2.8 Hz, 2H). ^{13}C NMR (100 MHz, $(CD_3)_2SO$) δ 155.2, 154.9, 137.1, 133.1, 132.1, 129.5, 125.9, 121.9, 121.5, 116.2, 115.6, 113.7, 113.6. LRMS m/z calcd for $C_{14}H_{11}N_3O_4SBr$ $[M + H]^+$ 396.0; found 396.8. Purity of the compound was further confirmed by RP-HPLC by using method 1: R_t = 7.98 min (98% pure; Supporting Information, Figure S2).

N-(Phenyl)-N-methyl-2,3-dioxo-1,2,3,4-tetrahydro-6-quinoxalinesulfonamide (31): As described for the synthesis of compound **29**, 2,3-dihydroxy-6-quinoxalinesulfonyl chloride (0.30 g, 1.15 mmol), *N*-methylaniline (0.25 mL, 2.30 mmol), and DMF (6 mL) were used to afford compound **31** (0.27 g, 71%) as a white solid. ^{1}H NMR (400 MHz, $(CD_3)_2SO$) δ 12.24 (s, 1H), 12.00 (s, 1H), 7.34 (d, J = 8.0 Hz, 2H), 7.31–7.29 (m, 2H), 7.22 (s, 1H), 7.20 (d, J = 1.6 Hz, 1H), 7.10 (m, 2H), 3.12 (s, 3H). ^{13}C NMR (100 MHz, $(CD_3)_2SO$) δ 155.2, 154.8, 141.1, 129.8, 129.6, 129.0, 127.4, 126.4, 125.9, 122.3, 120.0, 115.4, 114.5, 114.4, 38.0. LRMS m/z calcd for $C_{15}H_{14}N_3O_4S$ $[M + H]^+$ 332.1; found 332.8. Purity of the compound was further confirmed by RP-HPLC by using method 1: R_t = 8.20 min (99% pure; Supporting Information, Figure S3).

N-(Phenyl)-2,3-dioxo-1,2,3,4-tetrahydro-6-quinoxalinesulfonamide (32): As described for the synthesis of compound **29**, 2,3-dihydroxy-6-quinoxalinesulfonyl chloride (0.30 g, 1.15 mmol), aniline (0.21 mL, 2.30 mmol), and DMF (6 mL) were used to afford compound **32** (0.22 g, 61%) as a light-yellow solid. ^{1}H NMR (400 MHz, $(CD_3)_2SO$) δ 12.15 (s, 1H), 12.08 (s, 1H), 10.32 (br s, 1H), 7.53 (s, 1H), 7.44 (d, J = 8.4 Hz, 1H), 7.24–7.17 (m, 3H), 7.08 (d, J = 8.4 Hz, 2H), 7.02 (t, J = 7.2 Hz, 1H). ^{13}C NMR (100 MHz, $(CD_3)_2SO$) δ 155.2,

154.9, 137.6, 133.5, 129.3, 129.2, 125.8, 124.0, 121.5, 119.9, 115.5, 113.7. LRMS *m*/*z* calcd for $C_{14}H_{12}N_3O_4S$ $[M + H]^+$ 318.1; found 318.8. Purity of the compound was further confirmed by RP-HPLC by using method 1: R_t = 4.97 min (97% pure; Supporting Information, Figure S4).

N-(4-Isopropylphenyl)-N-methyl-2,3-dioxo-1,2,3,4-tetrahydro-6-quinoxalinesulfonamide (33): As described for the synthesis of compound **29**, 2,3-dihydroxy-6-quinoxalinesulfonyl chloride (0.30 g, 1.15 mmol), 4-isopropyl-*N*-methylaniline (0.34 g, 2.30 mmol), and DMF (6 mL) were used to afford compound **33** (0.20 g, 48%) as a white solid. ^{1}H NMR (400 MHz, $(CD_3)_2SO$) δ 12.25 (s, 1H), 12.00 (s, 1H), 7.34 (s, 1H), 7.23 (m, 1H), 7.21 (dt, *J* = 8.8, 2.4 Hz, 2H), 7.00 (dt, *J* = 8.8, 2.4 Hz, 2H), 3.09 (s, 3H), 2.88 (hep, *J* = 7.2 Hz, 1H), 1.18 (d, *J* = 7.2 Hz, 6H). ^{13}C NMR (100 MHz, $(CD_3)_2SO$) δ 155.2, 154.8, 147.5, 138.8, 130.2, 129.5, 126.8, 126.4, 125.9, 122.3, 115.5, 114.5, 114.4, 38.2, 33.0, 23.8. LRMS *m*/*z* calcd for $C_{18}H_{20}N_3O_4S$ $[M + H]^+$ 374.1; found 374.8. Purity of the compound was further confirmed by RP-HPLC by using method 1: R_t = 9.71 min (97% pure; Supporting Information, Figure S5).

N-(4-Isopropylphenyl)-2,3-dioxo-1,2,3,4-tetrahydro-6-quinoxalinesulfonamide (34): As described for the synthesis of compound **29**, 2,3-dihydroxy-6-quinoxalinesulfonyl chloride (0.30 g, 1.15 mmol), 4-isopropylaniline (0.31 g, 2.30 mmol), and DMF (6 mL) were used to afford compound **34** (0.24 g, 59%) as a pink solid. ^{1}H NMR (400 MHz, $(CD_3)_2SO$) δ 12.15 (s, 1H), 12.08 (s, 1H), 10.21 (br s, 1H), 7.52 (d, *J* = 2.0 Hz, 1H), 7.44 (dd, *J* = 8.4, 2.0 Hz, 1H), 7.18 (d, *J* = 8.4 Hz, 1H), 7.09 (app dt, *J* = 8.4, 2.0 Hz, 2H), 6.99 (app dt, *J* = 8.4, 2.0 Hz, 2H), 2.76 (hep, *J* = 6.8 Hz, 1H), 1.10 (d, *J* = 6.8 Hz, 6H). ^{13}C NMR (100 MHz, $(CD_3)_2SO$) δ 155.2, 155.0, 144.1, 135.2, 133.8, 129.3, 127.0, 125.8, 121.5, 120.3, 115.5, 113.75, 113.69, 32.7, 23.8. LRMS *m*/*z* calcd for $C_{17}H_{18}N_3O_4S$ $[M + H]^+$ 360.1; found 360.8. Purity of the compound was further confirmed by RP-HPLC by using method 1: R_t = 8.92 min (100% pure; Supporting Information, Figure S6).

N-(4-Chlorophenyl)-N-methyl-2,3-dioxo-1,2,3,4-tetrahydro-6-quinoxalinesulfonamide (35): As described for the synthesis of compound **29**, 2,3-dihydroxy-6-quinoxalinesulfonyl chloride (0.30 g, 1.15 mmol), 4-chloro-*N*-methylaniline (0.28 mL, 2.30 mmol), and DMF (6 mL) were used to afford compound **35** (0.16 g, 38%) as a white solid. ^{1}H NMR (400 MHz, $(CD_3)_2SO$) δ 12.26 (s, 1H), 12.00 (s, 1H), 7.42 (d, *J* = 8.8 Hz, 2H), 7.24 (d, *J* = 8.8 Hz, 2H), 7.23 (s, 1H), 7.12 (m, 2H), 3.09 (s, 3H). ^{13}C NMR (100 MHz, $(CD_3)_2SO$) δ 155.2, 154.8, 140.0, 131.7, 129.8, 129.3, 128.9, 128.6, 128.1, 125.9, 122.4, 115.5, 114.5, 37.8. LRMS *m*/*z* calcd for $C_{15}H_{13}ClN_3O_4S$ $[M + H]^+$ 366.0; found 366.8. Purity of the compound was further confirmed by RP-HPLC by using method 1: R_t = 8.32 min (95% pure; Supporting Information, Figure S7).

N-(2-Methoxyphenyl)-N-methyl-2,3-dioxo-1,2,3,4-tetrahydro-6-quinoxalinesulfonamide (36): As described for the synthesis of compound **29**, 2,3-dihydroxy-6-quinoxalinesulfonyl chloride (0.30 g, 1.15 mmol), 2-methoxy-*N*-methylaniline (0.31 mL, 2.30 mmol), and DMF (6 mL) were used to afford compound **36** (0.12 g, 29%) as a white solid. ^{1}H NMR (400 MHz, $(CD_3)_2SO$) δ 12.23 (s, 1H), 11.99 (s, 1H), 7.40 (d, *J* = 2.0 Hz, 1H), 7.38–7.34 (m,

1H), 7.33–7.30 (m, 1H), 7.24 (d, J = 8.4 Hz, 1H), 7.14 (dd, J = 8.0, 1.2 Hz, 1H), 7.01 (dd, J = 8.0, 1.2 Hz, 1H), 6.93 (td, J = 7.6, 1.2 Hz, 1H), 3.36 (s, 3H), 3.08 (s, 3H). ^{13}C NMR (100 MHz, $(CD_3)_2SO$) δ 156.2, 155.3, 154.9, 132.9, 131.0, 129.8, 129.2, 128.6, 125.7, 122.2, 120.4, 115.2, 114.2, 112.6, 55.2, 37.7. LRMS m/z calcd for $C_{16}H_{16}BrN_3O_5S$ $[M + H]^+$ 362.1; found 362.8. Purity of the compound was further confirmed by RP-HPLC by using method 1: R_t = 7.22 min (100% pure; Supporting Information, Figure S8).

N-(3-Fluorophenyl)-N-methyl-2,3-dioxo-1,2,3,4-tetrahydro-6-quinoxalinesulfonamide (37): As described for the synthesis of compound **29**, 2,3-dihydroxy-6-quinoxalinesulfonyl chloride (0.30 g, 1.15 mmol), 3-fluoro-*N*-methylaniline (0.26 mL, 2.30 mmol), and DMF (6 mL) were used to afford compound **37** (0.06 g, 15%) as a white solid. ^{1}H NMR (400 MHz, $(CD_3)_2SO$) δ 12.26 (s, 1H), 12.00 (s, 1H), 7.39 (app q, J = 8.0 Hz, 1H), 7.30 (s, 1H), 7.23 (m, 2H), 7.16 (td, J = 8.8, 5.6 Hz, 1H), 7.03 (dt, J = 10.8, 2.4 Hz, 1H), 6.99 (m, 1H), 3.12 (s, 3H). ^{13}C NMR (100 MHz, $(CD_3)_2SO$) δ 163.0, 160.6, 155.2, 154.8, 142.8, 142.7, 130.5, 130.4, 129.8, 129.4, 125.9, 122.3, 122.09, 122.06, 115.5, 114.4, 114.2, 114.0, 113.4, 113.1, 37.7. LRMS m/z calcd for $C_{15}H_{13}FN_3O_4S$ $[M + H]^+$ 350.1; found 350.8. Purity of the compound was further confirmed by RP-HPLC by using method 1: R_t = 7.38 min (100% pure; Supporting Information, Figure S9).

N-(3-Bromophenyl)-N-methyl-2,3-dioxo-1,2,3,4-tetrahydro-6-quinoxalinesulfonamide (38): As described for the synthesis of compound **29**, 2,3-dihydroxy-6-quinoxalinesulfonyl chloride (0.30 g, 1.15 mmol), 3-bromo-*N*-methylaniline (0.29 mL, 2.30 mmol), and DMF (6 mL) were used to afford compound **38** (0.02 g, 4%) as a white solid. ^{1}H NMR (400 MHz, $(CD_3)_2SO$) δ 12.27 (s, 1H), 12.01 (s, 1H), 7.51 (ddd, J = 7.6, 2.0, 1.2 Hz, 1H), 7.35 (t, J = 2.0 Hz, 1H), 7.32 (d, J = 8.0 Hz, 1H), 7.29 (m, 1H), 7.23 (m, 2H), 7.14 (ddd, J = 7.6, 2.0, 1.2 Hz, 1H), 3.11 (s, 3H). ^{13}C NMR (100 MHz, $(CD_3)_2SO$) δ 155.2, 154.8, 142.6, 130.8, 129.8, 129.3, 129.1, 129.0, 125.9, 125.1, 122.3, 121.3, 115.5, 114.5, 37.7. LRMS m/z calcd for $C_{15}H_{13}BrN_3O_4S$ $[M + H]^+$ 410.0; found 410.8. Purity of the compound was further confirmed by RP-HPLC by using method 1: R_t = 8.72 min (100% pure; Supporting Information, Figure S10).

N-(3-Methoxyphenyl)-N-methyl-2,3-dioxo-1,2,3,4-tetrahydro-6-quinoxalinesulfonamide (39): As described for the synthesis of compound **29**, 2,3-dihydroxy-6-quinoxalinesulfonyl chloride (0.20 g, 0.77 mmol), 3-methoxy-*N*-methylaniline (0.20 mL, 1.54 mmol), and DMF (4 mL) were used to afford compound **39** (0.05 g, 17%) as a gray solid. ^{1}H NMR (400 MHz, $(CD_3)_2SO$) δ 12.23 (s, 1H), 11.99 (s, 1H), 7.33 (d, J = 1.6 Hz, 1H), 7.27–7.22 (m, 3H), 6.88 (m, 1H), 6.67–6.65 (m, 2H), 3.70 (s, 3H), 3.11 (s, 3H). ^{13}C NMR (100 MHz, $(CD_3)_2SO$) δ 159.3, 155.1, 154.8, 142.2, 130.0, 129.60, 129.57, 125.8, 122.3, 118.2, 115.4, 114.4, 112.8, 112.3, 55.2, 38.0. LRMS m/z calcd for $C_{16}H_{16}N_3O_5S$ $[M + H]^+$ 362.1; found 362.8. Purity of the compound was further confirmed by RP-HPLC by using method 1: R_t = 7.56 min (98% pure; Supporting Information, Figure S11).

N-(3,5-Dimethoxyphenyl)-N-methyl-2,3-dioxo-1,2,3,4-tetrahy-dro-6-quinoxalinesulfonamide (40): As described for the synthesis of compound **29**, 2,3-dihydroxy-6-quinoxalinesulfonyl chloride (0.20 g, 0.77 mmol), 3,5-dimethoxy-*N*-

methylaniline (0.26 g, 1.54 mmol), and DMF (4 mL) were used to afford compound **40** (0.03 g, 10%) as a white solid. ^{1}H NMR (400 MHz, $(CD_3)_2SO$) δ 12.23 (s, 1H), 12.00 (s, 1H), 7.37 (d, J = 2.0 Hz, 1H), 7.29 (dd, J = 8.0, 2.0 Hz, 1H), 7.23 (d, J = 8.0 Hz, 1H), 6.45 (t, J = 2.0 Hz, 1H), 6.25 (d, J = 2.0 Hz, 2H), 3.67 (s, 3H), 3.65 (s, 3H), 3.09 (s, 3H). ^{13}C NMR (100 MHz, $(CD_3)_2SO$) δ 160.2, 155.2, 154.8, 142.8, 130.1, 129.6, 125.8, 122.3, 115.4, 114.4, 104.6, 99.1, 55.3, 38.0. LRMS m/z calcd for $C_{17}H_{18}N_3O_6S$ $[M + H]^+$ 392.1; found 392.8. Purity of the compound was further confirmed by RP-HPLC by using method 1: R_t = 8.17 min (95% pure; Supporting Information, Figure S12).

N-(3-Methylphenyl)-N-methyl-2,3-dioxo-1,2,3,4-tetrahydro-6-quinoxalinesulfonamide (41): As described for the synthesis of compound **29**, 2,3-dihydroxy-6-quinoxalinesulfonyl chloride (0.20 g, 0.77 mmol), 3-methyl-*N*-methylaniline (0.19 mL, 1.54 mmol), and DMF (4 mL) were used to afford compound **41** (0.15 g, 58%) as a white solid. ^{1}H NMR (400 MHz, $(CD_3)_2SO$) δ 12.23 (s, 1H), 11.98 (s, 1H), 7.32 (m, 1H), 7.24–7.20 (m, 3H), 7.11 (m, 1H), 6.96 (m, 1H), 6.85 (m, 1H), 3.09 (s, 3H), 2.27 (s, 3H). ^{13}C NMR (100 MHz, $(CD_3)_2SO$) δ 155.2, 154.8, 141.1, 138.3, 130.0, 129.5, 128.7, 128.0, 127.1, 125.8, 123.2, 122.3, 115.4, 114.4, 38.0, 20.8. LRMS m/z calcd for $C_{16}H_{16}N_3O_4S$ $[M + H]^+$ 346.1; found 346.8. Purity of the compound was further confirmed by RP-HPLC by using method 1: R_t = 8.01 min (99% pure; Figure S13).

N-(3-Ethylphenyl)-N-methyl-2,3-dioxo-1,2,3,4-tetrahydro-6-quinoxalinesulfonamide (42): As described for the synthesis of compound **29**, 2,3-dihydroxy-6-quinoxalinesulfonyl chloride (0.20 g, 0.77 mmol), 3-ethyl-*N*-methylaniline (0.21 g, 1.54 mmol), and DMF (4 mL) were used to afford compound **42** (0.20 g, 74%) as a white solid. ^{1}H NMR (400 MHz, $(CD_3)_2SO$) δ 12.23 (s, 1H), 11.98 (s, 1H), 7.30 (s, 1H), 7.25 (t, J = 8.8, 1H), 7.23 (s, 1H), 7.14 (d, J = 7.2 Hz, 1H), 6.89 (m, 2H), 3.10 (s, 3H), 2.55 (q, J = 8.0 Hz, 2H), 1.09 (t, J = 8.0 Hz, 3H). ^{13}C NMR (100 MHz, $(CD_3)_2SO$) δ 155.1, 154.8, 144.6, 141.1, 129.9, 129.5, 128.8, 126.9, 125.8, 123.7, 122.3, 115.4. 114.5, 38.1, 27.9, 15.4. LRMS m/z calcd for $C_{17}H_{18}N_3O_4S$ $[M + H]^+$ 360.1; found 360.8. Purity of the compound was further confirmed by RP-HPLC by using method 1: R_t = 8.84 min (99% pure; Supporting Information, Figure S14).

N-(3-Isopropylphenyl)-N-methyl-2,3-dioxo-1,2,3,4-tetrahydro-6-quinoxalinesulfonamide (43): As described for the synthesis of compound **29**, 2,3-dihydroxy-6-quinoxalinesulfonyl chloride (0.07 g, 0.27 mmol), 3-*i*-propyl-*N*-methylaniline (0.08 g, 0.54 mmol), and DMF (1.5 mL) were used to afford compound **43** (0.06 g, 60%) as a white solid. ^{1}H NMR (400 MHz, $(CD_3)_2SO$) δ 12.25 (s, 1H), 11.99 (s, 1H), 7.27 (d, J = 8.0 Hz, 1H), 7.26 (t, J = 8.0 Hz, 1H), 7.22 (d, J = 2.0 Hz, 1H), 7.21 (dd, J = 8.4, 1.6 Hz, 1H), 7.17 (dt, J = 8.0, 1.2 Hz, 1H), 6.92 (ddd, J = 8.0, 2.0, 1.2 Hz, 1H), 6.85 (t, J = 2.0 Hz, 1H), 3.10 (s, 3H), 2.81 (hep, J = 6.8 Hz, 1H), 1.10 (d, J = 6.8 Hz, 6H). ^{13}C NMR (100 MHz, $(CD_3)_2SO$) δ 155.2, 154.8, 149.3, 141.1, 129.9, 129.5, 128.8, 125.8, 125.5, 124.3, 124.2, 122.3, 115.4, 114.6, 38.1, 33.1, 23.6. LRMS m/z calcd for $C_{18}H_{19}N_3O_4S$ $[M + H]^+$ 373.1; found 373.8. Purity of the compound was further confirmed by RP-HPLC by using method 1: R_t = 9.46 min (98% pure; Supporting Information, Figure S15).

N-(3-Butylphenyl)-N-methyl-2,3-dioxo-1,2,3,4-tetrahydro-6-quinoxalinesulfonamide (44): As described for the synthesis of compound **29**, 2,3-dihydroxy-6-quinoxalinesulfonyl chloride (0.06 g, 0.25 mmol), 3-butyl-*N*-methylaniline (0.08 g, 0.49 mmol), and DMF (1.5 mL) were used to afford compound **44** (0.10 g, 100%) as a pink solid. ^{1}H NMR (400 MHz, $(CD_3)_2SO$) δ 12.26 (s, 1H), 11.98 (s, 1H), 7.27 (m, 1H), 7.25 (s, 1H), 7.22 (m, 2H), 7.11 (d, J = 8.0 Hz, 1H), 6.94 (m, 1H), 6.80 (t, J = 2.0 Hz, 1H), 3.11 (s, 3H), 1.42–1.37 (m, 3H), 1.24–1.17 (m, 3H), 0.82 (t, J = 7.6 Hz, 3H). ^{13}C NMR (100 MHz, $(CD_3)_2SO$) δ 155.2, 154.8, 143.2, 141.0, 129.9, 129.5, 128.7, 127.4, 125.9, 125.8, 124.1, 122.3, 115.4, 114.6, 38.1, 34.5, 33.0, 21.6, 13.8. LRMS m/z calcd for $C_{18}H_{19}N_3O_4S$ $[M + H]^+$ 373.1; found 373.8. Purity of the compound was further confirmed by RP-HPLC by using method 1: R_t = 10.35 min (98% pure; Supporting Information, Figure S16).

N-(3-t-Butylphenyl)-N-methyl-2,3-dioxo-1,2,3,4-tetrahydro-6-quinoxalinesulfonamide (45): As described for the synthesis of compound **29**, 2,3-dihydroxy-6-quinoxalinesulfonyl chloride (0.03 g, 0.13 mmol), 3-*t*-butyl-*N*-methylaniline (0.04 g, 0.27 mmol), and DMF (1 mL) were used to afford compound **45** (0.03 g, 58%) as a brown solid. ^{1}H NMR (400 MHz, $(CD_3)_2SO$) δ 12.25 (s, 1H), 11.99 (s, 1H), 7.32 (dt, J = 8.0, 1.6 Hz, 1H), 7.30–7.26 (m, 2H), 7.23 (m, 2H), 6.94 (t, J = 1.6 Hz, 1H), 6.92 (d, J = 1.6 Hz, 1H), 3.11 (s, 3H), 1.17 (s, 9H). ^{13}C NMR (100 MHz, $(CD_3)_2SO$) δ 155.1, 154.7, 151.5, 140.9, 129.9, 129.5, 128.6, 125.7, 124.3, 124.0, 123.3, 122.3, 115.4, 114.6, 38.2, 34.3, 30.8. LRMS m/z calcd for $C_{19}H_{21}N_3O_4S$ $[M + H]^+$ 387.1; found 387.8. Purity of the compound was further confirmed by RP-HPLC by using method 1: R_t = 9.92 min (95% pure; Supporting Information, Figure S17).

N-(2-Naphthyl)-N-methyl-2,3-dioxo-1,2,3,4-tetrahydro-6-quinoxalinesulfonamide (46): As described for the synthesis of compound **29**, 2,3-dihydroxy-6-quinoxalinesulfonyl chloride (0.20 g, 0.77 mmol), *N*-methyl-2-naphthylamine (0.24 g, 1.54 mmol), and DMF (4 mL) were used to afford compound **46** (0.16 g, 55%) as an orange solid. ^{1}H NMR (400 MHz, $(CD_3)_2SO$) δ 12.24 (s, 1H), 11.95 (s, 1H), 7.95–7.86 (m, 3H), 7.64 (d, J = 2.0 Hz, 1H), 7.52 (m, 2H), 7.31–7.29 (m, 2H), 7.23 (m, 2H), 3.22 (s, 3H). ^{13}C NMR (100 MHz, $(CD_3)_2SO$) δ 155.1, 154.8, 138.6, 132.9, 131.7, 129.8, 129.6, 128.5, 127.9, 127.5, 126.6, 126.4, 125.9, 124.9, 124.3, 122.4, 115.5, 114.4, 38.1. LRMS m/z calcd for $C_{19}H_{15}N_3O_4S$ $[M + H]^+$ 381.1; found 381.8. Purity of the compound was further confirmed by RP-HPLC by using method 1: R_t = 9.36 min (97% pure; Supporting Information, Figure S18).

N-(4-Methoxy-2-naphthyl)-N-methyl-2,3-dioxo-1,2,3,4-tetrahydro-6-quinoxalinesulfonamide (47): As described for the synthesis of compound **29**, 2,3-dihydroxy-6-quinoxalinesulfonyl chloride (0.09 g, 0.35 mmol), *N*-methyl-4-methoxy-2-naphthylamine (0.13 g, 0.70 mmol), and DMF (2 mL) were used to afford compound **47** (0.03 g, 21%) as a yellow solid. ^{1}H NMR (400 MHz, $(CD_3)_2SO$) δ 12.24 (s, 1H), 11.97 (s, 1H), 8.11–8.09 (m, 1H), 7.82–7.80 (m, 1H), 7.55–7.48 (m, 2H), 7.35 (d, J = 2.0 Hz, 1H), 7.31 (dd, J = 8.4, 2.0 Hz, 1H), 7.23 (d, J = 8.4 Hz, 1H), 7.20 (d, J = 1.2 Hz, 1H), 6.71 (d, J = 2.0 Hz, 1H), 3.87 (s, 3H), 3.21 (s, 3H). ^{13}C NMR (100 MHz, $(CD_3)_2SO$) δ 155.2, 154.9, 154.8, 139.1, 133.4, 129.9, 129.7, 127.8, 127.2, 125.9, 125.8, 123.7, 122.5, 121.3, 116.7, 115.4, 114.5, 103.9, 55.7, 38.2. LRMS m/z calcd for $C_{20}H_{17}N_3O_5S$ $[M + H]^+$ 411.1; found

411.8. Purity of the compound was further confirmed by RP-HPLC by using method 1: R_t = 9.94 min (98% pure; Supporting Information, Figure S19).

Biochemistry and Biology

Protein, Reagents, and Small-Molecule Libraries—Recombinant *Mtb* Eis protein (Eis_*Mtb*),[5] AAC(6′)-Ie/APH(2″)-Ia,[21] AAC(3)-IV,[21] and AAC(2′)-Ic[5] were expressed and purified as reported previously. All chemicals including 5′,5-dithiobis(2-nitrobenzoic acid) (DTNB), Tween 80, neomycin B (NEO), kanamycin A (KAN), acetyl-CoA (AcCoA), and chlorhexidine were purchased from Sigma-Aldrich (St. Louis, MO, USA). Albumin–dextrose–catalase (ADC) was from BD Biosciences (San Jose, CA, USA). The high-throughput screening (HTS) to identify inhibitors of the acetyltransferase activity of purified Eis_*Mtb* was carried out at the Center for Chemical Genomics (CCG, University of Michigan) against 123000 compounds from: (i) a ChemDiv library (120000), (ii) the BioFocus NCC library, and (iii) the MicroSource MS2000 library. All small molecules were dissolved in DMSO prior to testing. The immediate follow-up assays to confirm inhibition or triage of false positives were performed with hit compounds from fresh powders purchased from ChemDiv (San Diego, CA, USA). *Note*: All concentrations noted below are the final concentrations in the assays.

Eis Chemical Library Screening—HTS was performed as previously described.[12] Briefly, absorbance signal from the reaction of the enzymatically released CoASH with Ellman's reagent, DTNB, at 412 nm (ε_{412} = 14150 $M^{-1}cm^{-1}$) was used to monitor the acetylation by Eis_*Mtb*. The reactions (40 μL) contained Tris (50 mM, pH 8.0 adjusted at room temperature), Eis (0.25 μM), NEO (100 μM), AcCoA (40 μM), DTNB (0.5 mM), and library compounds (20 μM). Chlorhexidine (5 μM) and DMSO (0.5%) served as positive and negative controls, respectively. Plates were incubated at room temperature and read on a PHERAstar plate reader at 5 min after initiation of the reaction. The average Z' score for the HTS assay was 0.60.

Hit Validation—Hit compounds were defined as displaying 3-fold or stronger inhibition than the standard deviation (calculated for the inert compounds) in the HTS. These compounds were tested in triplicate. The compounds that exhibited reproducible inhibitory activity in two out of three trials were then tested in dose–response assays in the concentration range from 20 μM to 78 nM (generated by 2-fold dilutions of the compound stock), and Hill plots were obtained for all compounds displaying dose-dependent inhibition.

Inhibition Kinetics—Absorbance was measured on a SpectraMax M5 plate reader for the reaction mixtures in 96-well plates (Thermo Fisher Scientific). Measurements were taken every 30 s for 10 min. Compounds were first serially dissolved in Tris-HCl (50 mM, pH 8.0, containing 10% v/v DMSO). A mixture (50 μL) of Eis (1 μM), KAN (400 μM), and Tris-HCl (50 mM, pH 8.0) was added to the inhibitors (100 μL) and incubated for 10 min. Reactions were initiated by the addition of a mixture (50 μL) of DTNB (8 mM), AcCoA (2 mM), and Tris-HCl (50 mM, pH 8.0). All assays were performed in triplicate. IC_{50} values were calculated by curved fitting to a Hill plot with KaleidaGraph 3.6 software (Table 1 and Supporting Information, Figure S20).

Inhibitor Selectivity—To investigate the selectivity of our inhibitors toward Eis, compounds **39** and **46** were tested against three additional AAC enzymes: AAC(2′)-Ic, AAC(3)-IV, and AAC(6′)-Ie/APH(2″)-Ia. The conditions utilized for determination of IC_{50} values were also used here under the optimum conditions for each enzyme. Compounds **39** and **46** (200 μM to 100 pM) were dissolved in buffer (50 mM MES, pH 6.6, for AAC(6′)-Ie/APH(2″)-Ia and AAC(3)-IV and 100 mM sodium phosphate, pH 7.4, for AAC(2′)-Ic). Enzyme (0.25 μM for AAC(6′)-Ie/APH(2″)-Ia, 0.125 μM for AAC(3)-IV and AAC(2′)-Ic), NEO (100 μM), and AcCoA (150 μM) were used for these assays. AAC(3)-IV and AAC(2′)-Ic experiments were incubated at 25 °C. AAC(6′)-Ie/APH(2″)-Ia experiments were incubated at 37 °C. All other methods and concentrations are the same as for the experiments with Eis_*Mtb*.

Mycobacterial MIC Determination by Alamar Blue Assay—*Mtb* strains H37Rv and K204 were inoculated from frozen stocks into Middlebrook 7H9 broth supplemented with ADC (10%), Tween 80 (0.05%), and glycerol (0.4%) and incubated at 37 °C until turbidity appeared. The cultures were diluted with fresh 7H9 medium to the attenuance at 600 nm of 0.2, further diluted 1:25 in fresh 7H9 medium in 50 mL polypropylene tubes containing glass beads, and vortexed for 30 s. The cultures were kept still for 10 min, and then 90 μL aliquots were distributed into the wells of a clear 96-well culture plate. Compounds were tested at concentrations that were either 100-fold higher than their IC_{50} values in the enzyme assay or at 100 μM if the IC_{50} value could not be achieved while keeping the DMSO concentration ≤1% in test wells. Working stocks for each compound were prepared at concentrations twice that of the desired final concentration in fresh 7H9 medium, and 100 μL of each of these working stocks was added to the 90 μL of bacterial cultures in the wells. The plates were incubated at 37 °C for 24 h in a humid environment before the addition of KAN (10 μL). Growth of H37Rv was evaluated at 2.5 and 1.25 μg/mL KAN while growth of K204 was evaluated at 10, 5, 2.5, and 1.25 μg/mL KAN. The plates were incubated at 37 °C for 6 days after the addition of KAN. Then, 40 μL of Alamar blue diluted 1:2 in 10% Tween 80 was added to each well and the plates continued to be incubated 37 °C. The color of each well was preliminarily evaluated 24 h after the addition of Alamar blue, with a final evaluation after 48 h. Alamar blue changes from indigo blue to pink as a result of bacterial growth. The lowest concentration of KAN that resulted in no change in color was defined as the MIC for each concentration of an inhibitory compound. Compound screening was carried out on biological replicates in duplicate. Several controls were included with every compound: uninoculated 7H9, compound, and inoculated 7H9 only, inoculated 7H9 + DMSO only, and inoculated 7H9 only. For each plate, 200 μL of sterile water was added to all perimeter wells to minimize evaporation.

Structural Biology

Purification of EisC204A—The active point mutant EisC204A that is less prone to oxidation than the wild-type Eis_*Mtb* was overexpressed in BL21(DE3) *E. coli* and purified as previously reported,[7] with only minor modifications, as follows. The EisC204A-pET28a plasmid was transformed into *E. coli* BL21 (DE3) chemically competent cells and plated onto LB agar containing kanamycin (KAN; 50 μg/mL). After overnight incubation at 37 °C, a single colony from the plate was inoculated into LB broth (5 mL) containing KAN (50

μg/mL) (LB/KAN). This culture was grown at 37 °C until the attenuance at 600 nm of 0.5, then the culture was inoculated into 4 L of LB/KAN and grown at 37 °C. At the attenuance at 600 nm of ~0.1, the culture was transferred to 16 °C for 1.5 h, and then IPTG was added at the final concentration of 0.5 mM. The induced culture was grown for an additional 16–18 h at 16 °C with shaking (200 rpm). All following purification steps were done at 4 °C. The cells were pelleted by centrifugation at 5000 rpm for 10 min. The cell pellets were resuspended in chilled lysis buffer (NaCl (300 mM), Tris-HCl, pH 8.0, adjusted at room temperature (40 mM), glycerol (10% v/v), and β-mercaptoethanol (2 mM)). The cells were then disrupted by sonication, and the insoluble material was removed by centrifugation at 35000*g* for 45 min at 4 °C. The supernatant was passed through a 0.45 μm Millex-HV PVDF filter (Millipore, Billerica, MA, USA) and then loaded onto a 5 mL Ni-IMAC HisTrap FF column (GE Healthcare) pre-equilibrated in the lysis buffer. The column was washed with 100 mL of lysis buffer containing 20 mM imidazole, and then the protein was eluted in 10 mL of lysis buffer containing 200 mM imidazole. The eluate was concentrated using an Amicon Ultra-15 (10000 MWCO) centrifugal filter device (Millipore) to the volume of 5 mL. The protein was then purified on a size-exclusion S-200 column (GE Healthcare) equilibrated in gel filtration buffer (Tris-HCl pH 8.0 (40 mM), NaCl (100 mM), and β-mercaptoethanol (2 mM)). The Eis-containing fractions were pooled and concentrated using an Amicon Ultra (10000 MWCO) centrifugal filter device (Millipore) to 4 mg/mL. The pure Eis protein was stored on ice at 4 °C.

Crystallization, Diffraction Data Collection, and Structure Determination and Refinement of EisC204A-CoA-Inhibitor 39 Complex—Crystals were grown by vapor diffusion in hanging drops containing 1 μL of concentrated (4 mg/mL) EisC204A protein containing KAN (10 mM) and CoA (8 mM) mixed with 1 μL of the reservoir solution (Tris-HC,l pH 8.5, adjusted at room temperature (100 mM), PEG 8,000 (10–15% w/v), and $(NH_4)_2SO_4$ (0.4 M)). The drops were equilibrated against 1 mL of the reservoir solution at 22 °C. Single crystals were obtained in 2–3 weeks. The crystals were first gradually transferred into the reservoir solution. The $(NH_4)_2SO_4$ and KAN were then exchanged out of the solvent by a gradual transfer into the reservoir solution lacking $(NH_4)_2SO_4$: (Tris-HCl pH 8.5 (100 mM) and PEG 8,000 (13% w/v)). Then the crystals were gradually transferred into the cryoprotectant solution (Tris-HCl pH 8.5 (100 mM), PEG 8,000 (13% w/v), and glycerol (20% v/v)) and incubated in this solution for 10 min. Upon the incubation, the crystals were transferred in the inhibitor solution (the cryoprotectant solution containing 0.5 mM inhibitor) for 30 min, and then frozen in liquid nitrogen by quick immersion.

The X-ray diffraction data were collected at 100 K at synchrotron beamline 22-ID of the Advanced Photon Source at the Argonne National Laboratory (Argonne, IL). The data were processed with HKL2000.[26] The crystal form was the same as that of wild-type Eis-CoA-acetamide complex determined previously by our group (PDB 3R1K[5]) and contained one Eis monomer in the asymmetric unit, with the Eis hexamer generated by crystal symmetry operations. We used this crystal structure (without ligands or water molecules) as the starting point and performed rigid body refinement by Refmac,[27] with the Eis monomer as a single rigid-body domain. After the rigid body refinement, strong difference $F_o - F_c$ electron density for the inhibitor **39** molecule and a part of CoA was apparent, which allowed us to

readily build these molecules into the difference electron density with Coot program.[28] The structures of EisC204A-CoA-inhibitor **39** complex was iteratively built and refined using programs Coot[28] and Refmac,[27] respectively. The data collection and refinement statistics for the structures reported here are given in Table 2. The Eis-C204A-CoA-inhibitor **39** complex structure was deposited in the Protein Data Bank with the PDB accession number 5IV0.

Supplementary Material

Refer to Web version on PubMed Central for supplementary material.

Acknowledgments

This work was funded by a National Institutes of Health (NIH) grant AI090048 (S.G.-T.), a grant from the Center for Chemical Genomics (CCG) at the University of Michigan (S.G.-T.), a grant from the Firland Foundation (S.G.-T.), as well as by startup funds from the College of Pharmacy at the University of Kentucky (S.G.-T. and O.V.T.). We thank Steve Vander Roest, Martha Larsen, and Paul Kirchhoff (CCG, University of Michigan) for help with HTS. We thank the staff of Sector 22 (SER-CAT) of the Advanced Photon Source at the Argonne National Laboratories for their assistance with the remote X-ray diffraction data collection.

ABBREVIATIONS USED

AACs	AG acetyltransferases
AG	aminoglycoside
AMK	amikacin
DUSP16	dual-specificity protein phosphatase 16
Eis	enhanced intracellular survival
HTS	high-throughput screening
KAN	kanamycin A
MDR	multidrug-resistant
MKP-7	mitogen-activated kinase phosphatase-7
Mtb	*Mycobacterium tuberculosis*
SAR	structure–activity relationship
TOB	tobramycin
TB	tuberculosis
XDR	extensively drug-resistant

References

1. Global Tuberculosis Report 2014. World Health Organization; Geneva: 2014.

2. Zaunbrecher MA, Sikes RD Jr, Metchock B, Shinnick TM, Posey JE. Overexpression of the chromosomally encoded aminoglycoside acetyltransferase *eis* confers kanamycin resistance in *Mycobacterium tuberculosis*. Proc Natl Acad Sci U S A. 2009; 106:20004–20009. [PubMed: 19906990]
3. Campbell PJ, Morlock GP, Sikes RD, Dalton TL, Metchock B, Starks AM, Hooks DP, Cowan LS, Plikaytis BB, Posey JE. Molecular detection of mutations associated with first-and second-line drug resistance compared with conventional drug susceptibility testing of *Mycobacterium tuberculosis*. Antimicrob Agents Chemother. 2011; 55:2032–2041. [PubMed: 21300839]
4. Jnawali HN, Yoo H, Ryoo S, Lee KJ, Kim BJ, Koh WJ, Kim CK, Kim HJ, Park YK. Molecular genetics of *Mycobacterium tuberculosis* resistant to aminoglycosides and cyclic peptide capreomycin antibiotics in Korea. World J Microbiol Biotechnol. 2013; 29:975–982. [PubMed: 23329063]
5. Chen W, Biswas T, Porter VR, Tsodikov OV, Garneau-Tsodikova S. Unusual regioversatility of acetyltransferase Eis, a cause of drug resistance in XDR-TB. Proc Natl Acad Sci U SA. 2011; 108:9804–9808.
6. Tsodikov OV, Green KD, Garneau-Tsodikova S. A random sequential mechanism of aminoglycoside acetylation by *Mycobacterium tuberculosis* Eis protein. PLoS One. 2014; 9:e92370. [PubMed: 24699000]
7. Houghton JL, Biswas T, Chen W, Tsodikov OV, Garneau-Tsodikova S. Chemical and structural insights into the regioversatility of the aminoglycoside acetyltransferase Eis. ChemBioChem. 2013; 14:2127–2135. [PubMed: 24106131]
8. Chen W, Green KD, Tsodikov OV, Garneau-Tsodikova S. Aminoglycoside multiacetylating activity of the enhanced intracellular survival protein from *Mycobacterium smegmatis* and its inhibition. Biochemistry. 2012; 51:4959–4967. [PubMed: 22646013]
9. Green KD, Pricer RE, Stewart MN, Garneau-Tsodikova S. Comparative study of Eis-like enzymes from pathogenic and non-pagthogenic bacteria. ACS Infect Dis. 2015; 1:272–283. [PubMed: 27622743]
10. Pricer RE, Houghton JL, Green KD, Mayhoub AS, Garneau-Tsodikova S. Biochemical and structural analysis of amino-glycoside acetyltransferase Eis from *Anabaena variabilis*. Mol BioSyst. 2012; 8:3305–3313. [PubMed: 23090428]
11. Green KD, Biswas T, Chang C, Wu R, Chen W, Janes BK, Chalupska D, Gornicki P, Hanna PC, Tsodikov OV, Joachimiak A, Garneau-Tsodikova S. Biochemical and structural analysis of an Eis family aminoglycoside acetyltransferase from *Bacillus anthracis*. Biochemistry. 2015; 54:3197–3206. [PubMed: 25928210]
12. Green KD, Chen W, Garneau-Tsodikova S. Identification and characterization of inhibitors of the aminoglycoside resistance acetyltransferase Eis from *Mycobacterium tuberculosis*. ChemMedChem. 2012; 7:73–77. [PubMed: 21898832]
13. Chen W, Green KD, Garneau-Tsodikova S. Cosubstrate tolerance of the aminoglycoside resistance enzyme Eis from *Mycobacterium tuberculosis*. Antimicrob Agents Chemother. 2012; 56:5831–5838. [PubMed: 22948873]
14. Houghton JL, Green KD, Pricer RE, Mayhoub AS, Garneau-Tsodikova S. Unexpected *N*-acetylation of capreomycin by mycobacterial Eis enzymes. J Antimicrob Chemother. 2013; 68:800–805. [PubMed: 23233486]
15. Yoon HJ, Kim KH, Yang JK, Suh SW, Kim H, Jang S. A docking study of enhanced intracellular survival protein from *Mycobacterium tuberculosis* with human DUSP16/MKP-7. JSynchrotron Radiat. 2013; 20:929–932. [PubMed: 24121342]
16. Hugonnet JE, Tremblay LW, Boshoff HI, Barry CE 3rd, Blanchard JS. Meropenem-clavulanate is effective against extensively drug-resistant *Mycobacterium tuberculosis*. Science. 2009; 323:1215–1218. [PubMed: 19251630]
17. Willby MJ, Green KD, Gajadeera CS, Hou C, Tsodikov OV, Posey JE, Garneau-Tsodikova S. Potent inhibitors of acetyltransferase Eis overcome kanamycin resistance in *Mycobacterium tuberculosis*. ACS Chem Biol. 2016; 11:1639–1646. [PubMed: 27010218]

18. Garzan A, Willby MJ, Green KD, Tsodikov OV, Posey JE, Garneau-Tsodikova S. Discovery and optimization of two Eis inhibitor families as kanamycin adjuvants against drug-resistant. M tuberculosis ACS Med Chem Lett. 2016; doi: 10.1021/acsmedchemlett.6b00261
19. Ainsa JA, Perez E, Pelicic V, Berthet FX, Gicquel B, Martin C. Aminoglycoside 2′-*N*-acetyltransferase genes are universally present in mycobacteria: characterization of the *aac(2′)-Ic* gene from *Mycobacterium tuberculosis* and the *aac(2′)-Id* gene from *Mycobacterium smegmatis*. Mol Microbiol. 1997; 24:431–441. [PubMed: 9159528]
20. Vetting MW, Hegde SS, Javid-Majd F, Blanchard JS, Roderick SL. Aminoglycoside 2′-*N*-acetyltransferase from *Mycobacterium tuberculosis* in complex with coenzyme A and aminoglycoside substrates. Nat Struct Biol. 2002; 9:653–658. [PubMed: 12161746]
21. Green KD, Chen W, Houghton JL, Fridman M, Garneau-Tsodikova S. Exploring the substrate promiscuity of drug-modifying enzymes for the chemoenzymatic generation of *N*-acylated aminoglycosides. ChemBioChem. 2010; 11:119–126. [PubMed: 19899089]
22. Magalhaes ML, Blanchard JS. The kinetic mechanism of AAC3-IV aminoglycoside acetyltransferase from *Escherichia coli*. Biochemistry. 2005; 44:16275–16283. [PubMed: 16331988]
23. Boehr DD, Daigle DM, Wright GD. Domain-domain interactions in the aminoglycoside antibiotic resistance enzyme AAC(6′)-APH(2″). Biochemistry. 2004; 43:9846–9855. [PubMed: 15274639]
24. Caldwell SJ, Berghuis AM. Small-angle X-ray scattering analysis of the bifunctional antibiotic resistance enzyme aminoglyco-side (6′) acetyltransferase-Ie/aminoglycoside (2″) phosphotransferase-Ia reveals a rigid solution structure. Antimicrob Agents Chemother. 2012; 56:1899–1906. [PubMed: 22290965]
25. Obafemi C, Akinpelu D. Synthesis and antimicrobial activity of some 2(1H)-quinoxaline-6-sulfonyl derivatives. Phosphorus, Sulfur Silicon Relat Elem. 2005; 180:1795–1807.
26. Otwinowski Z, Minor W. Processing of X-ray diffraction data collected in oscillation mode. Methods Enzymol. 1997; 276:307–326.
27. Murshudov GN, Vagin AA, Dodson EJ. Refinement of macromolecular structures by the maximum-likelihood method. Acta Crystallogr, Sect D: Biol Crystallogr. 1997; 53:240–255. [PubMed: 15299926]
28. Emsley P, Cowtan K. Coot: model-building tools for molecular graphics. Acta Crystallogr, Sect D: Biol Crystallogr. 2004; 60:2126–2132. [PubMed: 15572765]
29. Laskowski RA, Macarthur MW, Moss DS, Thornton JM. Procheck - a program to check the stereochemical quality of protein structures. J Appl Crystallogr. 1993; 26:283–291.

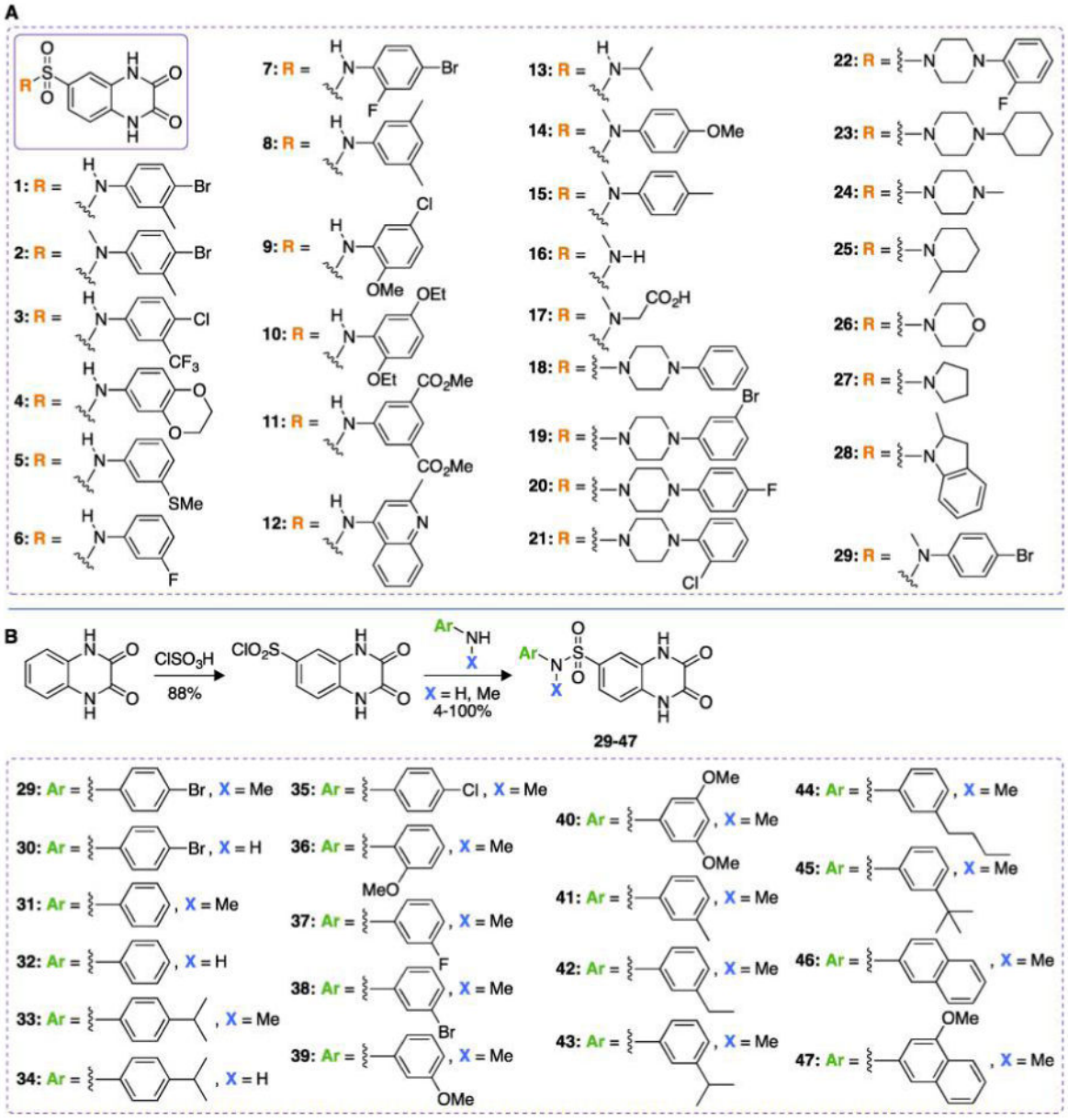

Figure 1.

(A) Structures of the sulfonamides (**1**–**29**) tested in the HTS campaign. (B) Synthetic scheme used for the preparation of the sulfonamide analogues **29**–**47** generated in this study.

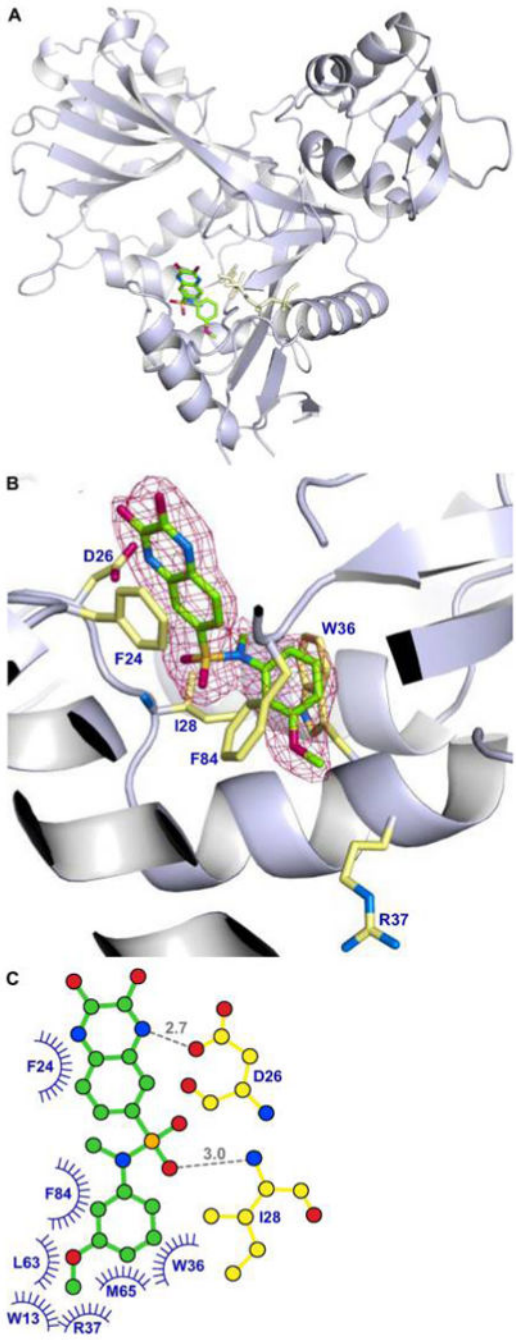

Figure 2.

Cartoon view of the crystal structure of Eis in complex with compound **39** and CoA. (A) Overall view of a monomer of Eis-CoA-inhibitor **39** complex. The ordered portion of the bound CoA, which does not directly interact with inhibitor **39**, is shown as very pale-yellow sticks; the rest of the CoA molecule is disordered. (B) Zoomed-in view of the AG-binding site with the bound inhibitor. The omit $F_o - F_c$ map (contoured at 3σ) generated without the inhibitor is shown as the red mesh. The inhibitor is shown as sticks (with carbon in green, nitrogen in blue, sulfur in orange, and oxygen in red), and the interacting side chains of Eis

are shown as pale-yellow sticks (with oxygen in red and nitrogen in blue). (C) A schematic of Eis-inhibitor **39** contacts. The hydrogen bonds are shown by dashed gray lines and the bond lengths are in Å. The residues involved in nonpolar interactions are shown by blue arcs.

Table 1

IC_{50} Values against Purified Eis and KAN MIC Values against *Mtb* H37Rv and *Mtb* K204 in the Absence and Presence of the Compounds at the Specified Concentrations

compd no.	Ar	X	IC_{50} (μM)[a]	concentration tested (μM)[b]	H37Rv MIC_{KAN} (μg/mL)[c]	K204 MIC_{KAN} (μg/mL)[d]
					1.25	10
29	*p*-Br-Ph	Me	0.08 ± 0.02	8	≤1.25	2.5
30	*p*-Br-Ph	H	6.2 ± 1.3	100	≤1.25	5
31	Ph	Me	5.8 ± 1.8	100	≤1.25	5
32	Ph	H	>200	100	≤1.25	10
33	*p*-*i*Pr-Ph	Me	0.25 ± 0.06	25	≤1.25	2.5-5
34	*p*-*i*Pr-Ph	H	10.6 ± 2.5	100	≤1.25	5
35	*p*-Cl-Ph	Me	0.100 ± 0.045	10	≤1.25	2.5
36	*o*-OMe-Ph	Me	>200	100	≤1.25	10
37	*m*-F-Ph	Me	3.0 ± 0.7	30	≤1.25	5
38	*m*-Br-Ph	Me	0.056 ± 0.004	5.6	≤1.25	2.5
39	*m*-OMe-Ph	Me	5.8 ± 1.2	100	≤1.25	≤1.25
40	3,5-di-OMe-Ph	Me	7.4 ± 3.3	100	≤1.25	5-10
41	*m*-Me-Ph	Me	0.37 ± 0.09	37	≤1.25	2.5-5
42	*m*-Et-Ph	Me	0.027 ± 0.012	2.7	≤1.25	5-10
43	*m*-*i*Pr-Ph	Me	0.23 ± 0.03	23	≤1.25	2.5-5
44	*m*-*n*Bu-Ph	Me	0.7 ± 0.3	70	≤1.25	5-10
45	*m*-*t*Bu-Ph	Me	27 ± 8	100	≤1.25	5-10
46	2-naphthyl	Me	0.00024 ± 0.00010	100	≤1.25	≤1.25
47	4-OMe-2-naphthyl	Me	0.30 ± 0.08	100	≤1.25	10

[a] IC_{50} values and standard errors for inhibition of purified Eis enzyme.

[b] Compounds were tested at concentrations that were either 100-fold higher than their IC_{50} or at 100 μM if the IC_{50} value could not be achieved while keeping the DMSO concentration at ≤1% in test wells. At these concentrations, the compounds did not inhibit the growth of *Mtb* H37Rv or that of *Mtb* K204 when tested in the absence of KAN.

[c] Anti-TB activity of KAN against *Mtb* H37Rv.

[d] Anti-TB activity of KAN against *Mtb* K204.

Table 2

X-ray Diffraction Data Collection and Refinement Statistics for the EisC204A-CoA-Inhibitor 39 Ternary Complex Structure (PDB 5IV0)

Data Collection	
space group	*R*32
no. of monomers per asymmetric unit	1
unit cell dimensions	
a, *b*, *c* (Å)	175.2, 175.2, 122.3
α, *β*, *γ* (deg)	90, 90, 120
resolution (Å)	50.0-2.1 (2.14-2.10)[a]
I/σ	16 (2.1)
completeness (%)	95.8 (97.7)
redundancy	3.9 (3.8)
R_{merge}	0.08 (0.50)
no. of unique reflections	37907
Structure Refinement Statistics	
resolution (Å)	40.0-2.1
R (%)	19.4
R_{free} (%)	21.9
bond length deviation (rmsd) from ideal (Å)	0.006
bond angle deviation (rmsd) from ideal (deg)	1.35
Ramachandran plot statistics[b]	
% of residues in most allowed regions	93.8
% of residues in additional allowed regions	6.2
% of residues in generously allowed regions	0.0
% of residues in disallowed regions	0.0 (0 residues)

[a] Numbers in parentheses indicate the values in the highest-resolution shell.

[b] Indicates Procheck statistics.[29]